Optimizing analysis of W-AlN cermet solar absorbing coatings

2001 J. Phys. D: Appl. Phys. 34 3113

(http://iopscience.iop.org/0022-3727/34/21/303)

INSTITUTE OF PHYSICS PUBLISHING JOURNAL OF PHYSICS D: APPLIED PHYSICS
J. Phys. D: Appl. Phys. **34** (2001) 3113–3120 PII: S0022-3727(01)24654-3

Optimizing analysis of W-AlN cermet solar absorbing coatings

Qi-Chu Zhang

School of Physics, The University of Sydney, NSW 2006, Australia

Received 9 May 2001, in final form 2 August 2001
Published 23 October 2001
Online at stacks.iop.org/JPhysD/34/3113

Abstract
The layer thickness and tungsten metal volume fraction of W-AlN cermet solar selective absorbing coatings on a W, Cu or Al infrared reflector with a surface aluminium oxynitride (AlON) or Al_2O_3 ceramic anti-reflector layer were optimized using physical modelling calculations. Due to limited published data for the refractive index of AlN, and likely oxygen contamination during reactive sputtering of AlN ceramic materials, AlON was used as the ceramic component and the published value of its refractive index was employed. The dielectric function and then the complex refractive index of W-AlON cermet materials were calculated using the Ping Sheng approximation. The downhill simplex method in multi-dimensions was used in the numerical calculation to achieve maximum photo-thermal conversion efficiency at 350 °C under a concentration factor of 30 for a solar collector tube. Optimization calculation results show that the initial graded (ten-step layers) cermet films all converge to something close to a three-layer film structure, which consists of a low metal volume fraction cermet layer on a high metal volume fraction cermet layer on a metallic infrared reflector with a surface ceramic anti-reflection layer. The optimized three-layer solar coatings have a high solar absorptance of 0.95 for AlON and 0.96 for the Al_2O_3 anti-reflection layer, and a low hemispherical emittance of 0.073 at 350 °C. For the optimized three-layer films the solar radiation is efficiently absorbed internally and by phase interference. Thermal loss is very low for optimized three-layer films due to high reflectance values in the thermal infrared wavelength range and a very sharp edge between low solar reflectance and high thermal infrared reflectance. The high metal volume fraction cermet layer has a metal-like optical behaviour in the thermal infrared wavelength range and makes the largest contribution to the increase of emittance compared with that of the metal infrared reflector.

1. Introduction

Solar thermal electricity systems utilize solar radiation to generate electricity via the photo-thermal conversion method. The solar thermal electricity technology using a parabolic trough has been commercialized. The silver reflection surface of a parabolic trough concentrates sunlight onto a solar collection tube located along the trough's focal line, which absorbs solar radiation and converts it to thermal energy. Despite its technical success, the cost of solar thermal electricity still exceeds that of conventional electricity generation. The solar collector tubes and silver solar parabolic reflectors are the two main contributions to the extra investment costs, and considerable effort has been spent trying to reduce these costs.

The solar collection tube consists of an inner tube and a glass envelope, and the space between them is evacuated to eliminate thermal conductance loss. The outside surface of the inner tube was coated with a Mo-Al_2O_3 cermet solar selective surface for solar thermal electricity applications, which has excellent thermal stability at a high operating temperature of 380–500 °C [1]. A planar magnetron sputter

coater was used to deposit the Mo-Al_2O_3 cermet solar selective surface onto a tube substrate using conventional sputtering technology. The Mo metal component in the cermet was deposited by running a Mo metal target using direct current (dc) sputtering, and the Al_2O_3 ceramic component was deposited by running an Al_2O_3 ceramic target using radio frequency (rf) sputtering. For the planar rf-sputtered ceramic component, the deposition rate is lower and the cost of deposition equipment is much higher compared with dc reactive sputtering. The deposition of Mo-Al_2O_3 cermet solar coatings is therefore much more expensive than dc reactive sputtered SS-C and Al-N cermet solar coatings, which are also mass-produced using a commercial-scale cylindrical dc sputtering coater and are widely applied in solar hot water heaters [2–5]. The Mo-Al_2O_3 cermet layer was made with a graded metal concentration, which approaches its percolation point at the bottom and is zero at the top of the cermet layer. The graded cermet film structure was first proposed by Ritchie and Window in 1977 [6]. The optical reflectance of the composite absorber layer in the solar radiation range is reduced by increasing the metal volume fraction from the surface to the bottom [6, 7]. Through fundamental analysis we proposed that cermet solar coatings with a double cermet layer film structure, incorporating two distinct cermet layers rather than a conventional graded cermet layer, may have the highest solar performance [8–11].

Recently, we have studied a series of new cermet materials for solar selective coatings deposited by dc magnetron sputtering technology. This invention has two main innovative features: (1) the ceramic and metallic components in the cermet are simultaneously deposited by dc sputtering; (2) the ceramic component is deposited by dc reactive sputtering and the metallic component by dc non-reactive sputtering. We have deposited W-AlN cermet solar selective coatings using the above sputtering technology that have very good thermal stability at high temperature in vacuum [12, 13]. A solar absorptance of 0.92–0.94 and a normal emittance of 0.03–0.04 at room temperature were achieved. In this paper we describe an optimization study of the W-AlN cermet solar coatings using a physical model.

2. Physical model for optimization of cermet solar coatings

An ideal solar selective absorbing coating absorbs most incident solar radiation while simultaneously suppressing thermal emittance loss. Commonly quoted parameters of performance for solar absorbing coatings are solar absorptance and thermal emittance. The angular-dependent solar absorptance α and thermal emittance ε are defined, respectively, by

$$\alpha(\theta) = \int_0^\infty \mathrm{d}\lambda\, A(\lambda)[1 - R(\theta,\lambda)] \Big/ \int_0^\infty \mathrm{d}\lambda\, A(\lambda) \qquad (1)$$

$$\varepsilon(\theta, T) = \int_0^\infty \mathrm{d}\lambda\, E(T,\lambda)[1 - R(\theta,\lambda)] \Big/ \int_0^\infty \mathrm{d}\lambda\, E(T,\lambda) \qquad (2)$$

were $A(\lambda)$ is the spectral solar radiance and $E(T,\lambda)$ the spectral blackbody emissive power. $R(\theta,\lambda)$ is the angular-dependent spectral reflectance. The hemispherical emittance is given by

$$\varepsilon_h(t) = \int_0^{\pi/2} \mathrm{d}\theta \sin(2\theta) \int_0^\infty \mathrm{d}\lambda\, E(T,\lambda)[1 - R(\theta,\lambda)] \Big/ \int_0^\infty \mathrm{d}\lambda\, E(T,\lambda). \qquad (3)$$

A commonly quoted photo-thermal conversion efficiency is given by [14]

$$\eta = \alpha - \varepsilon_h \sigma T^4 / CI \qquad (4)$$

where σ is the Stefan–Boltzmann constant. C and I are the flux amplification or concentration factor, and solar flux intensity, respectively.

W-AlN cermet solar coatings would be most suitable in solar collector tube applications. In this study a modified photo-thermal conversion efficiency for solar collector tubes is used,

$$\eta = B\alpha - \varepsilon_{eff}\sigma(T_1^4 - T_2^4)/CI \qquad (5)$$

where the parameter B is related to the transmittance of the glass envelope. The quantity ε_{eff} is the effective emittance, which, for two cylindrical specular surfaces, is often given by [15]

$$\varepsilon_{eff}(T_1, T_2) = \frac{1}{1/\varepsilon_{h,1}(T_1) + 1/\varepsilon_{h,2}(T_2) - 1} \qquad (6)$$

where $\varepsilon_{h,1}$ is the hemispherical emittance of the solar coatings at temperature T_1 and $\varepsilon_{h,2}$ is the hemispherical emittance of the glass envelope at temperature T_2. The precise photo-thermal conversion efficiency for solar collector tubes is given by [16]

$$\eta = B\alpha - (1/CI)\int_0^{\pi/2} \mathrm{d}\theta \sin(2\theta) \times \int_0^\infty \mathrm{d}\lambda \frac{E(T_1,\lambda) - E(T_2,\lambda)}{1/\varepsilon_1(T_1,\theta,\lambda) + 1/\varepsilon_2(T_2,\theta,\lambda) - 1}. \qquad (7)$$

If the refractive indices of the metal, ceramic and cermet materials are known, one can calculate the reflectance, then the solar absorptance, emittance and photo-thermal efficiency of the solar selective coatings. The refractive index of cermet materials can be calculated from the refractive indices of metal and ceramic components using a physical model. A model widely used for the dielectric function of a composite was proposed by Bruggeman (BR) [17]. For identical spherical grains with size much less than the wavelength of light, the average dielectric function of a composite in the Bruggeman approximation, ζ^{BR}, is given by [17, 18]

$$f_a \frac{\zeta_a - \zeta^{BR}}{\zeta_a + 2\zeta^{BR}} + (1 - f_a)\frac{\zeta_b - \zeta^{BR}}{\zeta_b + 2\zeta^{BR}} = 0 \qquad (8)$$

where ζ_a and ζ_b are the dielectric functions of metal (a) and ceramic (b), respectively. The filling factor f_a represents the volume fraction occupied by the metal spheres having ζ_a. The BR formula is self-consistent for a two-component mixture in which there are no distinguishable inclusions embedded in a defined matrix.

The BR theory predicts a percolation threshold, but it does not produce an optical dielectric anomaly. Ping Sheng (SH) [19] in 1980 proposed a modified theory to deal with the dielectric function of composites in order to obtain

good agreement with given experimental results. SH theory displays both the optical dielectric anomaly and the percolation threshold. The SH approximation works well in some cermets, even though at 50–60% high metal volume fractions [18–21]. In the SH approximation a probabilistic growth model for grains in a composite film has been introduced. The film is modelled as a mixture of two types of coated oblate spheroidal units, dielectric-coated metal spheroids described as type-a units and metal-coated dielectric spheroids described as type-b units. For the simple case of spherical grains, the relative probability of the occurrence for type-a units at any metal volume fraction is given by

$$J_a = \frac{(1 - f_a^{1/3})^3}{(1 - f_a^{1/3})^3 + [1 - (1 - f_a)^{1/3}]^3}. \tag{9}$$

For type-b units, $J_b = 1 - J_a$. For spherical grains the average dielectric function of a composite in Sheng's approximation, ζ^{SH}, is given by [18]

$$\begin{aligned} &J_a[(\zeta_b - \zeta^{SH})(\zeta_a + 2\zeta_b) + f_a(2\zeta_b + \zeta^{SH})(\zeta_a - \zeta_b)] \\ &\quad\times[(\zeta_b + 2\zeta^{SH})(\zeta_a + 2\zeta_b) + 2f_a(\zeta_b - \zeta^{SH})(\zeta_a - \zeta_b)]^{-1} \\ &\quad+J_b[(\zeta_a - \zeta^{SH})(\zeta_b + 2\zeta_a) \\ &\quad+(1 - f_a)(2\zeta_a + \zeta^{SH})(\zeta_b - \zeta_a)] \\ &\quad\times[(\zeta_a + 2\zeta^{SH})(\zeta_b + 2\zeta_a) \\ &\quad+2(1 - f_a)(\zeta_a - \zeta^{SH})(\zeta_b - \zeta_a)]^{-1} = 0. \end{aligned} \tag{10}$$

Here we rewrite an analogous formula to the Bruggeman approximation equation (8) by

$$J_b\frac{\zeta_1 - \zeta^{SH}}{\zeta_1 + 2\zeta^{SH}} + (1 - J_b)\frac{\zeta_2 - \zeta^{SH}}{\zeta_2 + 2\zeta^{SH}} = 0 \tag{11}$$

where

$$\zeta_1 = \zeta_a\frac{(2\zeta_a + \zeta_b) - 2(1 - f_a)(\zeta_a - \zeta_b)}{(2\zeta_a + \zeta_b) + (1 - f_a)(\zeta_a - \zeta_b)} \tag{12}$$

$$\zeta_2 = \zeta_b\frac{(\zeta_a + 2\zeta_b) + 2f_a(\zeta_a - \zeta_b)}{(\zeta_a + 2\zeta_b) - f_a(\zeta_a - \zeta_b)}. \tag{13}$$

The complex refractive index $n + \mathrm{i}k$, is derived from the complex dielectric function $\zeta = \zeta' + \mathrm{i}\zeta''$ using the relationship $n + \mathrm{i}k = \zeta^{1/2}$.

A matrix formulation approach, derived from the basic principles of Maxwell's equations, was used to calculate the reflectance for this special multi-layer system [22]. The solar absorptance is calculated using the calculated normal reflectance spectrum in the solar radiation region 0.3–2.5 μm and the Air Mass 1.5 spectrum. The emittance is found from the calculated spectral reflectance in the thermal infrared region 1–50 μm and the spectral blackbody emissive power. In the optimization calculations, the downhill simplex method in multi-dimensions [23] has been used to achieve maximum photo-thermal conversion efficiency.

3. Results

3.1. AlON/W-AlON/W solar coatings

The above physical model was used to optimize the metal volume fraction and layer thickness for the W-AlN cermet solar coatings. There are very limited published data for the refractive index of AlN [24]. Dc reactively sputtered aluminium nitride films generally contain oxygen owing to reaction with residual water vapour and oxygen in the chamber during the sputtering process [25]. Hence, AlON and tungsten were used as the ceramic and metal components in the cermet, respectively, and the published values for their refractive index were employed [26, 27]. The dielectric functions of W-AlON cermet materials were calculated using the SH approximation.

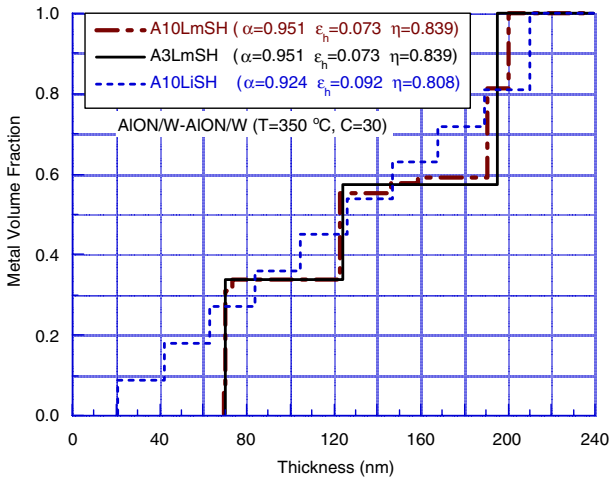

Figure 1. Optimized film structures of AlON/W-AlON/W solar coating for achieving maximum photo-thermal conversion efficiency for a solar collector tube at 350 °C with a concentration factor of 30 using the SH approximation of the dielectric function of W-AlON cermet materials. The full line is an optimized film structure for a three-layer film A3LmSH. The dot-dashed line represents an optimized ten-layer film A10LmSH. The initial ten-layer graded film A10LiSH (ten-step dashed line) used in the optimization is also included for comparison.

W-AlN cermet solar coatings have good thermal stability properties at high temperature in vacuum. They may be used for solar thermal electricity generation applications. Therefore, this optimization calculation was carried out assuming an elevated temperature and a high concentration. The modified photo-thermal conversion efficiency η for solar collector tubes, equation (5), was used in the numerical calculations. The value of parameter B was chosen to be 0.91, corresponding to the transmittance of borosilicate glass. The effective emittance was calculated using equation (6). The hemispherical emittance of envelope glass ε_{h2} was 0.85. The temperature of the glass envelope, T_2, was set at 20 °C. Figure 1 shows the optimized film structures for AlON/W-AlON/W solar coatings at 350 °C under a concentration factor of 30 for a solar collector tube. The dashed line represents an initial ten-layer (graded) film A10LiSH, from which the optimizing calculation started, and the dot-dashed line represents the optimized film structure A10LmSH of the ten-layer film. The full line represents the optimized three-layer film A3LmSH. For the ten-layer (graded) selective surfaces there are 19 parameters, one for the thickness of the ceramic anti-reflection layer and 18 for the cermet layers, nine for thicknesses and nine for metal volume fractions. It is clearly shown that the optimized ten-layer structure converges to something very close to a three-layer film. Both the optimized ten-layer film A10LmSH and the three-layer film

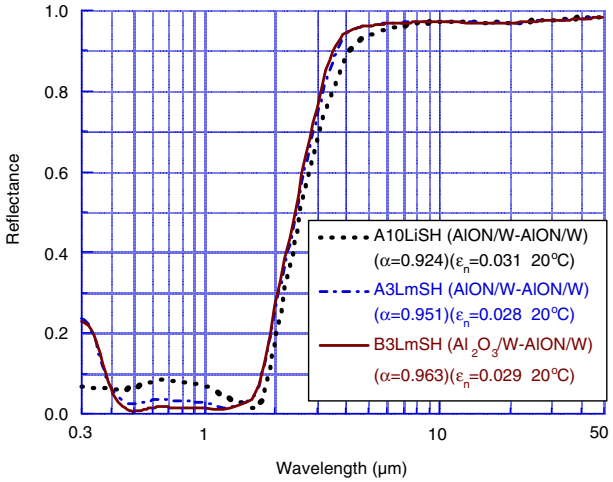

Figure 2. Three calculated normal reflectance spectra for the W-AlON solar selective coatings using the SH approximation of the dielectric function of cermet materials; the dashed curve represents the initial ten-layer graded film A10LiSH, the dot-dashed curve the optimized three-layer film A3LmSH and the full curve the optimized three-layer film B3LmSH. The layer thickness and metal volume fraction of these films is shown in figures 1 and 4.

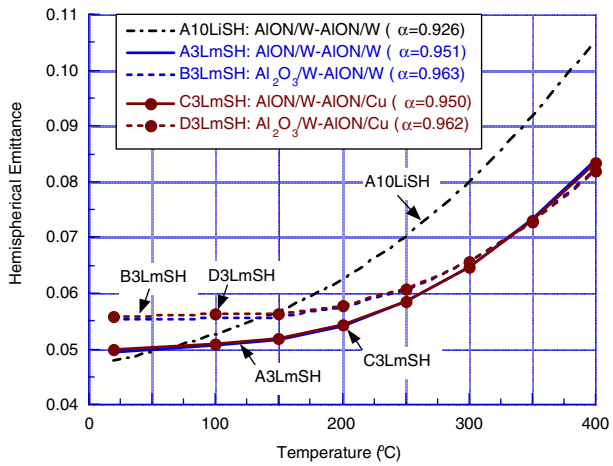

Figure 3. The temperature dependence of the calculated hemispherical emittance for a ten-layer graded film A10LiSH (dot-dashed curve), and four optimized three-layer films: A3LmSH (full curve), B3LmSH (dashed curve), C3LmSH (full curve with full circles) and D3LmSH (dashed curve with full circles) of the W-AlON cermet solar coatings.

A3LmSH have identical photo-thermal conversion efficiencies of 0.839, identical solar absorptances of 0.951 and identical hemispherical emittances of 0.073 at 350 °C. In comparison with the graded film A10LiSH, the solar absorptance increases by 0.027 and the hemispherical emittance reduces by 0.018. This indicates that the W-AlON cermet solar coating with a double cermet layer structure of two cermet layers on a W metal infrared reflector with a surface AlON ceramic anti-reflection layer has maximum photo-thermal conversion efficiency.

Figure 2 shows the calculated normal reflectance spectra for the W-AlON cermet solar coatings. The dashed curve is for the initial ten-layer (graded) film A10LiSH with a W metal volume fraction step value of 0.09 and a thickness step value of 21 nm. The dot-dashed curve corresponds to the optimized three-layer film A3LmSH which has W metal volume fractions of 0.341 for a relative low metal volume fraction (LMVF) cermet layer and 0.575 for a relative high metal volume fraction (HMVF) cermet layer. The layer thickness is 71 nm for the AlON anti-reflection layer, 53 nm for the LMVF layer and 68 nm for the HMVF layer as indicated in figure 1. These two reflectance spectra correspond to a solar absorptance of 0.924 and 0.951 and a normal emittance of 0.092 and 0.073 at 350 °C, respectively. The reflectance values of the three-layer film A3LmSH in the wavelength range 0.4–1.5 μm are lower than those of the graded ten-step film A10LiSH, which results in the solar absorptance increasing by 0.027. The reflectance values for wavelengths greater than 4 μm are very high, resulting in low emittance. The edge between the low solar reflectance and the high thermal infrared reflectance is very sharp, which also contributes to a relatively low emittance at elevated temperature, as shown in figure 3. It can be seen from figure 3 that the hemispherical emittances at room temperature are nearly identical for the initial graded film A10LiSH and the optimized three-layer film A3LmSH. However, the emittance of the graded film A10LiSH rises rapidly with temperature, from 0.048 at room temperature to 0.106 at 400 °C.

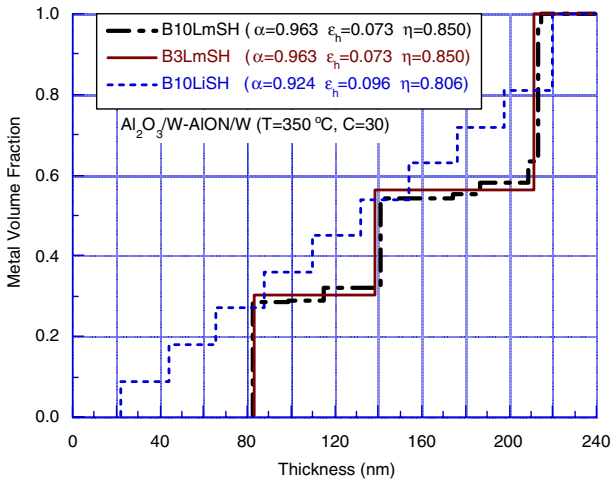

Figure 4. Optimized film structures of Al_2O_3/W-AlON/W selective surfaces at 350 °C with a concentration factor of 30 for a solar collector tube using the SH approximation of the dielectric function of cermet materials. The full line represents the optimized three-layer film B3LmSH, the dot-dashed line the optimized ten-layer film B10LmSH and the dashed line the initial ten-step graded film B10LiSH.

3.2. Al_2O_3/W-AlON/W solar coatings

An optimization study was also carried out for W-AlON cermet solar coatings with an Al_2O_3 anti-reflection layer. The published value for the refractive index of Al_2O_3 was employed [28]. Figure 4 shows the optimized film structure of a ten-layer film B10LmSH (dot-dashed line) at 350 °C under a concentration factor of 30 for a solar collector tube using the SH approximation of the dielectric function of W-AlON cermet materials. It also converges to one very close to a three-layer film B3LmSH. Both the optimized ten-layer film B10LmSH and the three-layer film B3LmSH have identical photo-thermal conversion efficiencies of 0.850, identical solar absorptances of 0.963 and identical hemispherical emittances of 0.073 at 350 °C. In comparison with the AlON anti-reflection layer,

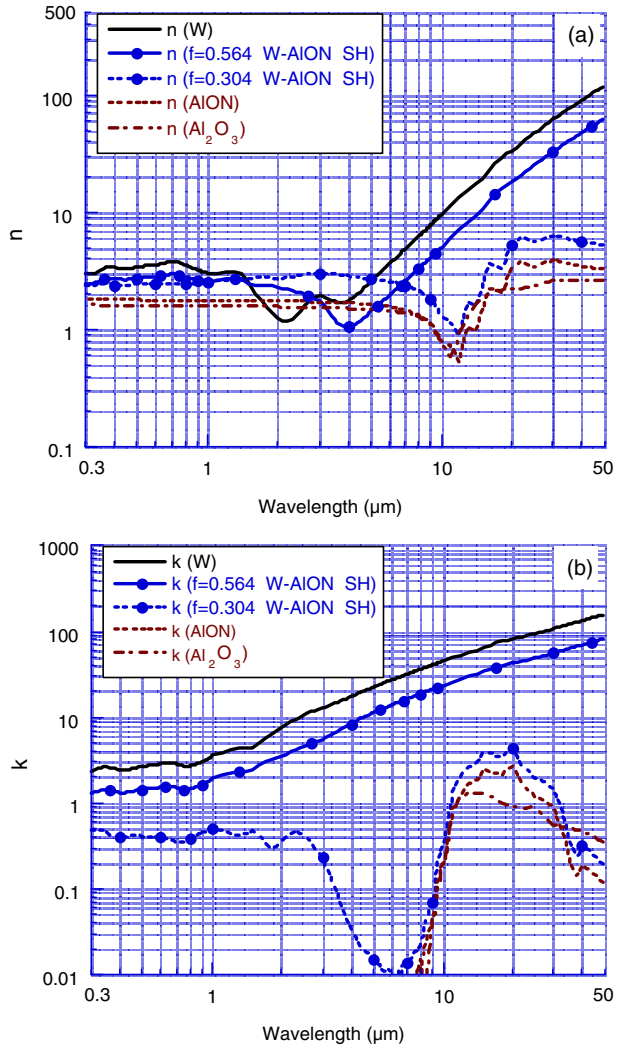

Figure 5. The wavelength dependence of the complex refractive indices $n + ik$, (a) for n and (b) for k, of the W-AlON cermet with W metal volume fraction 0.564 (full curve with full circles) and 0.304 (dashed curve with full circles) calculated using the SH approximation. The refractive indices of W (full curve), AlON (dashed curve) and Al_2O_3 (dot-dashed curve) are also included for comparison.

the solar absorptance increases by 0.012. The relatively low refractive index of Al_2O_3 in the main solar radiation spectrum region shown in figure 5 results in a lower reflectance as shown in figure 2, and then a solar absorptance increase. The optimized film has relatively lower metal volume fractions for the two cermet layers compared with the AlON anti-reflection layer. The temperature dependence of the calculated hemispherical emittance for the film B3LmSH is shown in figure 3.

Figure 5 shows the refractive index $n + ik$ of the W-AlON cermet with W metal volume fraction 0.564 and 0.304 corresponding to those for the optimized three-layer film B3LmSH as shown in figure 4, calculated using the SH approximation. The refractive indices of W, AlON and Al_2O_3 are also included for comparison. The k values of the LMVF ($f_W = 0.304$) W-AlON cermet are in the range 0.3–0.5 in the main solar radiation region. In the infrared AlON absorption region (peak value at 20 μm) the k values have a very similar

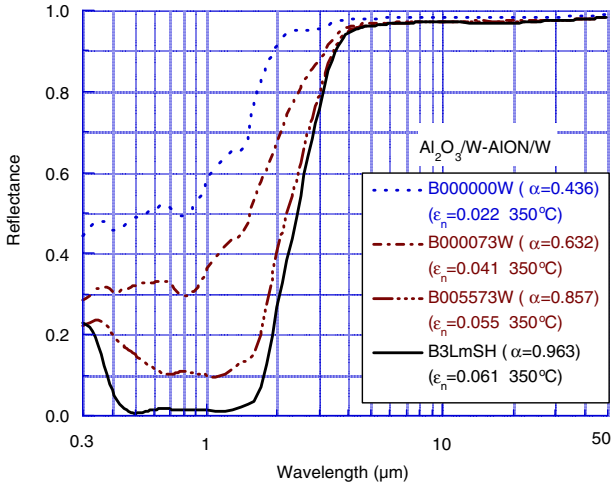

Figure 6. Two reflectance spectra of film B005573W (three-dot-dashed curve) for two cermet layers on a W reflector and film B000073W (dot-dashed curve) for a HMVF cermet layer on the W reflector. The thickness and metal volume fraction correspond to those for optimized Al_2O_3/W-AlON/W film B3LmSH. The spectra for film B3LmSH (full curve) and film B000000W (dashed curve) for the W reflector are also included for comparison.

pattern of variation to that of AlON, and are slightly higher than those of AlON. The k values of the HMVF ($f_W = 0.563$) W-AlON cermet have an identical very similar pattern of variation to that of metallic tungsten, and are nearly equal to half the value of those for W metal in the wavelength range 0.3–50 μm. The k values are in the range 1.2–2.0 in the wavelength range 0.3–1 μm, and then increase monotonically, finally reaching 83 at 50 μm.

Figure 6 shows the two calculated reflectance spectra of films B000073W and B005573W. The B000073W film corresponds to a HMVF cermet layer with $f_W = 0.564$ and $d = 73$ nm on a W infrared reflector. The B005573W film corresponds to a LMVF layer with $f_W = 0.304$ and $d = 55$ nm overlying the above HMVF cermet layer on a W infrared reflector. These thicknesses and metal volume fractions correspond to those for the optimized three-layer film B3LmSH. The spectra for the optimized film B3LmSH and film B000000W for the W reflector (dashed curve) are also included for comparison. The plot clearly shows the contribution of each layer to the reflectance value—in particular, to the reduction in reflectance in the main solar radiation region. For the film B000073W, a HMVF cermet layer on a W metal reflector the solar absorptance reaches 0.632 from 0.436 for W; when adding another LMVF cermet layer the solar absorptance reaches 0.867 and then further adding an Al_2O_3 anti-reflection layer increases the solar absorptance to 0.963.

3.3. AlON/W-AlON/Cu solar coatings

The thermal emittance may be further reduced by using a lower emittance material such as copper that is easy to sputter with good quality [29]. Therefore, an optimization study was conducted for a Cu infrared reflector layer with an AlON anti-reflection layer. The published value for the refractive index of copper was used [27]. The optimized ten-layer film

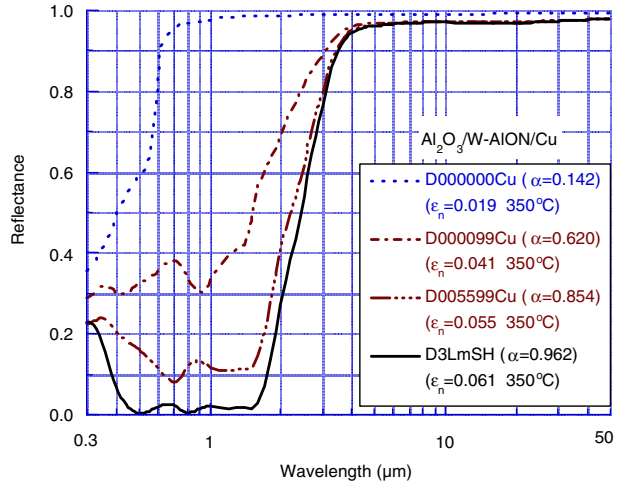

Figure 7. Two calculated reflectance spectra of film D005599Cu (three-dot-dashed curve) for two cermet layers on a Cu reflector and film D000099Cu (dot-dashed curve) for a HMVF cermet layer on a Cu reflector. The spectra for film D3LmSH (full curve) and film D000000Cu (dashed curve) for the Cu reflector are also included for comparison.

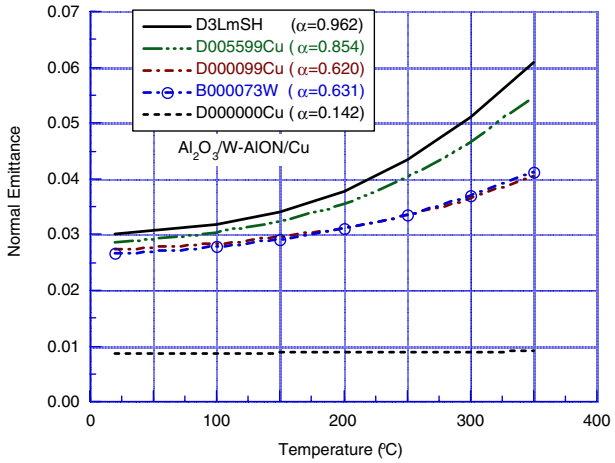

Figure 8. The temperature dependence of calculated normal emittance for four films, D3LmSH (full curve), D005599Cu (three-dot-dashed curve), D000099Cu (dot-dashed curve) and D000000Cu (dashed curve). The emittance for film B0000073W (dot-dashed curve with open circles) is also included for comparison.

also converges to something close to the optimized three-layer film C3LmSH. The optimized three-layer film C3LmSH has a nearly identical photo-thermal conversion efficiency of 0.838, a nearly identical solar absorptance of 0.950 and an identical hemispherical emittance of 0.073 at 350 °C to those for the optimized ten-layer film. The temperature dependence of the calculated hemispherical emittance for the film C3LmSH is shown in figure 3.

3.4. Al_2O_3/W-AlON/Cu solar coatings

An optimization study was also carried out for the W-AlON cermet solar coatings with Al_2O_3 anti-reflection material and Cu infrared reflector. The optimized ten-layer film also converges to something close to the optimized three-layer film D3LmSH. The optimized three-layer film D3LmSH has a nearly identical photo-thermal conversion efficiency of 0.849, a nearly identical solar absorptance of 0.962 and a nearly identical hemispherical emittance of 0.073 at 350 °C to those for the optimized ten-layer film. The temperature dependence of the calculated hemispherical emittance for the film D3LmSH is shown in figure 3.

Figure 7 shows the two calculated reflectance spectra of the films D000099Cu and D005599Cu. The D000099Cu film corresponds to a HMVF W-AlON cermet layer with $f_W = 0.573$ and $d = 99$ nm on a Cu infrared reflector. The D005599Cu film corresponds to a LMVF cermet layer with $f_W = 0.311$ and $d = 55$ nm overlying the above HMVF cermet layer on a Cu infrared reflector. These thicknesses and metal volume fractions correspond to those for the optimized three-layer film D3LmSH. The spectra for the optimized film D3LmSH (full curve) and the film D000000Cu for the Cu reflector (dashed curve) are also included for comparison. The plot clearly shows the contribution of each layer to the reflectance value—in particular, to the reduction in reflectance in the main solar radiation region. For the film D000099Cu, a HMVF cermet layer on the Cu metal reflector, the solar absorptance reaches 0.620 from 0.142 for Cu; when adding another LMVF cermet layer the solar absorptance reaches 0.854 and then further adding an Al_2O_3 anti-reflection layer increases the solar absorptance to 0.962.

Figure 8 shows the temperature dependence of the calculated normal emittance for the above four films, D3LmSH, D005599Cu, D000099Cu and D000000Cu. The emittance for film B0000073W with W infrared reflector is also included for comparison. It shows the contribution of each layer (HMVF and LMVF cermets as well as the Al_2O_3 anti-reflection layer) to the increase in emittance.

3.5. AlON/W-AlON/Al and Al_2O_3/W-AlON/Al solar coatings

Optimization studies were also carried out for the W-AlON cermet solar coatings with AlON and Al_2O_3 anti-reflection materials and Al infrared reflection at 350 °C under a concentration factor of 30 for a solar collector tube using the SH approximation of the dielectric function of the cermet. The published value for the refractive index of Al was employed [30]. The results of the numerical calculation also show that the three-layer film exhibits the maximum photo-thermal conversion efficiency. The layer thickness, the W metal volume fraction and the solar performance of the optimized three-layer films E3LmSH for AlON and F3LmSH for the Al_2O_3 anti-reflection layer are given in table 1.

4. Summary and discussion

Optimization calculation results show that the initial graded (ten-step layers) films for W-AlON cermet layers on a W, Cu or Al infrared reflector with an AlON or Al_2O_3 anti-reflection layer all converge to something close to a three-layer film structure—ceramic/W-AlON(LMVF)/W-AlON(HMVF)/metal. The optimized three-layer films have identical or nearly identical solar absorptance, hemispherical emittance and photo-thermal conversion efficiency to those of the corresponding optimized original graded cermet layer (ten-step layers) films. This is another new example confirming

Table 1. Summarized layer thickness and W metal volume fraction as well as the solar performance for the optimized three-layer films of the W-AlON cermet solar coatings using the SH approximation of the dielectric function of cermet materials.

Film	Film structure	Thickness (nm) (f_w)[a]	α	ε_h (350 °C)	η (350 °C, $C = 30$)
A3LmSH	AlON/W-AlON/W	71/53(0.341)/68(0.575)/W	0.951	0.073	0.839
B3LmSH	Al_2O_3/W-AlON/W	83/55(0.304)/73(0.564)/W	0.963	0.073	0.850
C3LmSH	AlON/W-AlON/Cu	71/53(0.343)/90(0.581)/Cu	0.950	0.073	0.838
D3LmSH	Al_2O_3/W-AlON/Cu	83/55(0.311)/99(0.573)/Cu	0.962	0.073	0.849
E3LmSH	AlON/W-AlON/Al	71/53(0.344)/91(0.583)/Al	0.950	0.073	0.838
F3LmSH	Al_2O_3/W-AlON/Al	83/55(0.311)/99(0.574)/Al	0.962	0.072	0.849

[a] The value in parentheses is the W metal volume fraction.

our proposal put forward in 1992 that solar selective coatings with a double cermet layer film structure have better solar performance than those with a one cermet layer or graded cermet layer film structures [8–11]. The layer thickness, W metal volume fraction and solar performance for the optimized three-layer films of the W-AlON cermet solar coatings are summarized in table 1. For the optimized three-layer film A3LmSH with structure AlON/W-AlON/W the solar absorptance reaches 0.95, an increase of 0.025 compared with the value of 0.924 for the graded film A10LiSH. Its hemispherical emittance at 350 °C is 0.073, a reduction of 0.019 compared with the value of 0.092 for the graded film.

For the optimized three-layer films the solar radiation is efficiently absorbed internally and by phase interference. This is verified by the following facts. The reflectance spectra of the optimized three-layer films, A3LmSH, B3LmSH, C3LmSH, D3LmSH, E3LmSH and F3LmSH, all have very low values and several minima and maxima in the main solar radiation wavelength region, as shown for example in figures 2 and 7. The solar absorptance reaches 0.95 for AlON and 0.96 for Al_2O_3 anti-reflection material. Figures 6 and 7 clearly show the contribution of the HMVF and LMVF cermet layer as well as the anti-reflection layer to the solar absorptance. For the films B000073W and D000099Cu, a HMVF cermet layer on a W or Cu metal reflector, the solar absorptance reaches 0.62–0.63 from 0.44 for W and from 0.14 for Cu; adding another LMVF cermet layer, the solar absorptance reaches 0.85–0.86. Further adding an Al_2O_3 anti-reflection layer causes the solar absorptance the increase to 0.96. The optimized three layer films, B3LmSH, D3LmSH and F3LmSH, with an Al_2O_3 anti-reflection layer yield an anti-reflection layer thickness of 81 nm and W metal volume fraction of ∼0.31 for the LMVF layer. These values are significantly different from those of the films A3LmSH, C3LmSH and E3LmSH using an AlON anti-reflection layer, which yield an anti-reflection layer thickness of 71 nm and W metal volume fraction of ∼0.34 for the LMVF layer. These variations are for matching reflection index reduction of the Al_2O_3 anti-reflection layer. However, the optical path of the anti-reflection layer is nearly identical for both the AlON and Al_2O_3 anti-reflection layers. In addition, the results from this study show that the solar absorptance is nearly independent of different infrared reflection materials, W, Cu or Al. Therefore, one can obtain very high solar absorptance, 0.95–0.96 or even 0.97, by optimizing the layer thickness and metal volume fraction of the two cermet layers as well as the layer thickness of the anti-reflection layer for any infrared reflector materials.

Thermal loss is very low for the optimized three-layer films due to the high reflectance values in the thermal infrared wavelength range shown in figures 2, 6 and 7, which are close to those of the W metal infrared reflector. The edge between the low solar reflectance and the high thermal infrared reflectance for the optimized three-layer films is very sharp and this results in a smaller slope for the increase in emittance with temperature than that for the graded films shown in figure 3. The LMVF layer has low W metal volume fraction 0.30–0.34, which is less than the percolation threshold, very low extinction k values for wavelengths greater than 4 μm, as shown in figure 5, and a thin layer thickness ∼55 nm. So this layer is nearly fully transparent for wavelengths greater than 4 μm, the same as for the ceramic anti-reflection layer. Therefore, the LMVF cermet layer can be considered as a ceramic-like material in the thermal infrared wavelength range. The HMVF cermet layer has high W metal volume fraction 0.56–0.58, which is greater than the percolation threshold, and then high k values nearly equal to half the value of the W metal in the infrared region. Therefore, this HMVF layer has metal-like optical behaviour and makes the largest contribution to the increase in emittance at room temperature compared with those of the metal infrared reflector. The contribution of the LMVF cermet layer and ceramic anti-reflection layer to the increase in emittance at room temperature is very low, being only around 0.002. However, their contributions to the emittance at 350 °C are high, being around 0.015 and 0.007, respectively. This increase in emittance is due to a lower reflectance in the wavelength range 1–4 μm and a blackbody radiation peak moving to short wavelengths with increasing temperature. Another interesting result is that the emittance of the optimized films is nearly independent of the type of infrared reflector, W, Cu or Al, as shown in figure 3 and table 1; nevertheless, the emittance of Cu is lower than that of W. In order to explain this result we calculated the reflectance for an interface between air and the HMVF cermet. The calculated reflectance has values of around 0.95 for wavelengths greater than 4 μm (not given in this paper). This is due to the high values of n and k of the HMVF W-AlON cermet material. Consider a light beam incident on a bare HMVF W-AlON cermet layer with $f_w = 0.56$–0.58 and $d = 68$–88 nm on a W or Cu metal reflector. Around 0.95 of the incident intensity is reflected at the surface for wavelengths greater than 4 μm, transmitting only 0.05. 0.8–0.9 of this transmitting beam is absorbed by the HMVF cermet layer. The intensity reaching the cermet/metal infrared reflector interface is only around 0.01. Therefore, the back-reflected beam makes a very small contribution to the overall reflectance, and so the choice of reflector, W, Cu or Al, will have little inference on the overall reflection. The difference in emittance between the films B000074W and D000099Cu, shown in figure 8, is less than 0.002. If one wishes to predict more precise results

for the emittance at an elevated operating temperature, the temperature dependence of emittance for metallic W may be considered. This should be studied further in the future.

5. Conclusions

We have carried out optimization studies for W-AlN cermet solar coatings with different anti-reflection and different infrared reflection materials using a physical numerical model. Due to limited published data for the refractive index of AlN, and likely oxygen contamination during reactive sputtering of AlN ceramic materials, aluminium oxynitride (AlON) was used as the ceramic component and a published value of its refractive index was employed. The dielectric function and then the complex refraction index of W-AlON cermet materials were calculated using the SH approximation. The downhill simplex method in multi-dimensions was used in the numerical calculation to achieve maximum photo-thermal conversion efficiency at 350 °C under a concentration factor of 30 for a solar collector tube. Optimization calculation results show that the initial graded (ten-step layers) films, consisting of W-AlON cermet layers on a W, Cu or Al infrared reflector with a surface AlON or Al_2O_3 anti-reflection layer, all converge to something close to a three-layer film structure—ceramic/W-AlON(LMVF)/W-AlON(HMVF)/metal. The optimized three-layer solar coatings have a high solar absorptance of 0.95 for AlON and of 0.96 for the Al_2O_3 anti-reflection layer, and a low hemispherical emittance of 0.073 at 350 °C. For a HMVF cermet layer on a metal reflector, the solar absorptance reaches 0.62–0.63 from 0.44 for W and from 0.14 for Cu; adding another LMVF cermet layer, the solar absorptance reaches 0.85–0.86. Further adding a Al_2O_3 anti-reflection layer causes the solar absorptance to increase to 0.96. The solar absorptance is nearly independent of infrared reflection material W, Cu or Al. Therefore, one can obtain a very high solar absorptance of 0.95–0.96 or even 0.97 by optimizing the layer thickness and metal volume fraction of the two cermet layers as well as the layer thickness of the anti-reflection layer for any infrared reflector material. Thermal loss is very low for optimized three-layer films due to high reflectance values in the thermal infrared wavelength range and a very sharp edge between the low solar reflectance and the high thermal infrared reflectance. For wavelengths greater than 4 μm the LMVF cermet layer is nearly full transparent; therefore, it can be considered as a ceramic-like material. The contribution of the LMVF cermet layer and ceramic anti-reflection layer to the emittance at room temperature is very low, being only around 0.002. The HMVF layer has a metal-like optical behaviour in the thermal infrared wavelength range and makes the largest contribution to the increase in emittance at room temperature compared with the results of the metal infrared reflector. Furthermore, the emittance of the optimized films is nearly independent of the infrared reflector W, Cu or Al, despite the emittance of Cu being lower than that of W. However, the W-AlON cermet solar coatings with a W infrared reflector layer have better thermal stability at high temperature compared with Cu or Al infrared reflector layers.

Acknowledgments

The author wishes to acknowledge the financial assistance of the Australian Research Council and His Royal Highness Prince Nawaf Bin Abdul Aziz of the Kingdom of Saudi Arabia through the Science Foundation for Physics within the University of Sydney.

References

[1] Lanxner M and Elgat Z 1990 *Proc. SPIE* **1272** 240
[2] Harding G L, Window B, McKenzie D R, Collins A R and Horwitz C M 1979 *J. Vac. Sci. Technol.* **16** 2105
[3] Window B and Harding G L 1984 *Solar Energy* **32** 609
[4] Yin Zhiqiang and Harding G L 1984 *Thin Solid Films* **120** 81
[5] Zhang Q-C, Zhao K, Zhang B-C, Wang L-F, Shen Z-L, Lu D-Q, Xie D-L and Li B-F 1999 *J. Vac. Sci. Technol.* A **17** 2885
[6] Ritchie I T and Window B 1977 *Appl. Opt.* **16** 1438
[7] Window B, McKenzie D and Harding G 1981 *Solar Energy Mater.* **2** 149
[8] Zhang Q-C and Mills D R 1992 *Appl. Phys. Lett.* **60** 545
[9] Zhang Q-C and Mills D R 1992 *J. Appl. Phys.* **72** 3013
[10] Zhang Q-C and Mills D R 1992 *Solar. Energy Mater. Sol. Cells* **27** 273
[11] Zhang Q-C, Mills D R and Monger A, The University of Sydney 1994 *Australia Patent* 646172
Zhang Q-C, Mills D R and Monger A 1996 *USA Patent* 5523132
[12] Zhang Q-C 1997 *J. Vac. Sci. Technol.* A **15** 2842
[13] Zhang Q-C 1998 *J. Phys. D: Appl. Phys.* **31** 355
[14] Trotter D M and Sievers A J 1980 *Appl. Opt.* **19** 771
[15] Siegel R and Howell J R 1972 *Thermal Radiation Heat Transfer* (New York: McGraw-Hill) ch 9
[16] Zhang Q-C, Simko T M, Dey C J, Collins R E, Turner G M, Brunotte M and Gombert A 1997 *Int. J. Heat Mass Transfer.* **40** 61
[17] Bruggeman D A G 1935 *Ann. Phys.* **24** 636
[18] Niklasson G A and Granqvist C G 1991 Selectively solar-absorbing surface coatings: optical properties and degradation *Materials Science for Solar Energy Conversion Systems* ed C G Granqvist (Oxford: Pergamon) p 70
[19] Sheng P 1980 *Phys. Rev. Lett.* **45** 60
[20] Perrin J, Despax B and Kay E 1985 *Phys. Rev.* B **32** 719
[21] Martinu L 1987 *Solar Energy Mater.* **15** 21
[22] Zhang Q-C, Kelly J C and Mills D R 1990 *J. Appl. Phys.* **68** 4788
[23] Press W H, Flannery B P, Teukolsky S A and Vetterling W T 1986 *Numerical Recipes, The Art of Scientific Computing* (Cambridge: Cambridge University Press) p 289
[24] Solanki A K, Kashyap A, Nautiyal T, Auluck S and Khan M A 1995 *Solid State Commun.* **94** 1009
[25] Lee H-C, Kim G-H, Hong S-K, Lee K-Y, Yong Y-J, Chun C-H and Lee J-Y 1995 *Thin Solid Films* **261** 148
[26] Tropf W J and Thomas M E 1991 Aluminium oxynitride (ALON) spinel *Handbook of Optical Constants of Solids II* ed E D Palik (New York: Academic) p 777
[27] Lynch D W and Hunter W R 1985 Comments on the optical constants of metals and an introduction to the data for several metals *Handbook of Optical Constants of Solids* ed E D Palik (New York: Academic) p 275
[28] Gervais F 1991 Aluminium oxide (Al_2O_3) *Handbook of Optical Constants of Solids II* ed E D Palik (New York: Academic) p 761
[29] Window B and Harding G L 1981 *J. Opt. Soc. Am.* **71** 354
[30] Smith D Y, Shiles E and Inokuti M 1985 The optical properties of metallic aluminum *Handbook of Optical Constants of Solids* ed E D Palik (New York: Academic) p 369